Available online at www.sciencedirect.com
ScienceDirect
Journal of Sound and Vibration 303 (2007) 305–329
JOURNAL OF SOUND AND VIBRATION
www.elsevier.com/locate/jsvi

Features of dynamic response sensitivity and its application in damage detection

Z.R. Lu[a], S.S. Law[b,*]

[a]Department of Applied Mechanics and Engineering, Zhongshan University, Guangzhou, 510275, People's Republic of China
[b]Civil and Structural Engineering Department, Hong Kong Polytechnic University, Hunghom, Kowloon, Hong Kong, People's Republic of China

Received 19 April 2006; received in revised form 4 July 2006; accepted 19 January 2007
Available online 7 March 2007

Abstract

The sensitivity of general dynamic response of a structure with respect to a perturbation in a parameter of a dynamic system is addressed in this paper. The sensitivities of response of the structure when under sinusoidal, impulsive and random excitations is calculated, and their properties discussed. Local damage in the structure is represented by a perturbation of a system parameter, and a new sensitivity-based approach is presented for identifying the local damages in a structure directly from the measured dynamic responses. The solution is obtained with the penalty function method iteratively with regularization. Simulation studies on the effectiveness and accuracy of the proposed method are performed including measurement noise and initial model errors, and experiment work on steel beams with local damages has also been conducted. The proposed method is seen to give acceptable results even with the different types of model errors taking advantage of the plentiful amount of measured data from the responses.

1. Introduction

Due to unforeseen conditions and circumstances, it is never possible to design and build a structure that is not liable of failure. Structural aging, adverse environmental effects, etc. are examples affecting the safety and reliability of a structure. Regular inspection and condition assessment of an engineering structure are necessary so that early detection of any defect can be made, and the safety and reliability of the structure can be determined. Early damage identification allows maintenance and repair works to be properly programmed and thus minimizing the maintenance costs.

Many researchers have presented methods for damage identification using natural frequencies and mode shapes, including the sensitivity methods [1–7], optimization methods [8], modal residual methods [9–12], wavelet transform methods [13–18] and modal force error methods [19,20]. More recently, Liu and Chen [21] presented a computational inverse technique for identifying stiffness distribution in structures using structural

*Corresponding author.
E-mail address: cesslaw@polyu.edu.hk (S.S. Law).

0022-460X/$ - see front matter © 2007 Elsevier Ltd. All rights reserved.
doi:10.1016/j.jsv.2007.01.021

dynamic response in the frequency domain, where the sensitivity matrix of displacement amplitude with respect to the stiffness factor was calculated by Newton's method.

In the damage identification of structures, the damage parameters are generally related to the stiffness as discussed by Araujo dos Santos et al. [5], Bicanic and Chen [2] and Chen and Bicanic [3]. When discretizing the structure into a number of finite elements, the stiffness distribution in the structures is expressed in terms of the stiffness parameters. One of the main difficulties in identifying the stiffness parameters lies in the large number of unknowns. When solving an inverse problem of parameter identification, it is usually formulated as an objective function of a weighted sum of squared difference between the measured value and the corresponding simulated value of the dynamic properties of the structures. The inverse reconstruction can then be solved by minimizing the objective function. Genetic algorithms (GAs) have been widely used as a searching technique for such nonlinear problem. The advantages of GAs lie in, (a) they do not need the sensitivity analysis and initial guess [22–24]; and (b) they converge to the global optimum solution. However, the disadvantage of GAs is computationally extensive and they suffer from slow convergence at the later stage due to the nature of random searching. Thus, for problems with large number of parameters to be identified, the use of GA becomes less practical.

This paper addresses the problem of insufficient measured data for the identification of a dynamic system with a larger number of unknowns. Dynamic response can be measured at all accessible degrees-of-freedoms (dof) of a structure, and the amount of data is only limited with time. It is directly used in the proposed method as an unlimited source of damage information in the damage detection problem. The sensitivity matrix of dynamic response of a structure with respect to a perturbation of a system parameter is addressed. An error function, defined as the difference between the calculated and measured responses of the structure, is used in the sensitivity equation for the system identification problem. Penalty function method is used for the iterative solution with regularization. The sensitivities of the dynamic responses with respect to the unknown parameters are then calculated to form the sensitivity matrix. Computation simulation with a plane frame structure and the European Space Agency Structure illustrate the effectiveness and accuracy of the proposed method. Satisfactory results can be obtained even when the measured data is polluted with noise and with initial model error. Experimental results from two steel beams in the laboratory also demonstrate the advantage of the plentiful amount of dynamic response data and the accuracy of the proposed method.

2. Forward problem

2.1. Dynamic response of the structure

For a general finite element model of a linear elastic time-invariant structure, the equation of motion is given by

$$[M]\{\ddot{d}\} + [C]\{\dot{d}\} + [K]\{d\} = [B]\{F\}, \tag{1}$$

where $[M]$, $[C]$ and $[K]$ are the system mass, damping and stiffness matrices respectively. Rayleigh damping is adopted which is of the form $[C] = a_1[M] + a_2[K]$, where a_1 and a_2 are constants to be determined from two modal damping ratios. If a more accurate estimation of the actual damping is required, a more general form of Rayleigh damping, the Caughey damping model [25] can be adopted. $\{\ddot{d}\}$, $\{\dot{d}\}$ and $\{d\}$ are the acceleration, velocity and displacement response vectors of the structure, $\{F\}$ is a vector of applied forces with matrix $[B]$ mapping these forces to the associated dof of the structure. The dynamic responses of the structures can be obtained by direct numerical integration using Newmark method.

2.1.1. Sensitivity of response in time domain

For the perturbation of a system parameter, $\Delta\alpha$, the perturbed equation of motion is obtained by differentiating both sides of Eq. (1) with respect to the system parameter. Assuming the parameter is related only to the stiffness of the dynamic system, we have,

$$[M]\left\{\frac{\partial \ddot{d}}{\partial \alpha^i}\right\} + [C]\left\{\frac{\partial \dot{d}}{\partial \alpha^i}\right\} + [K]\left\{\frac{\partial d}{\partial \alpha^i}\right\} = -\frac{\partial [K]}{\partial \alpha^i}\{d\} - a_2\frac{\partial [K]}{\partial \alpha^i}\{\dot{d}\} \quad (i = 1, 2, \ldots N), \tag{2a}$$

where $\{\partial d/\partial \alpha^i\}$, $\{\partial \dot{d}/\partial \alpha^i\}$, $\{\partial \ddot{d}/\partial \alpha^i\}$ are vectors of the displacement, velocity and acceleration sensitivities with respect to the unknown parameter. α^i is the parameter in the ith element or other stiffness parameter of the system. Similar equation can be written for the perturbation of parameters which are related to the system mass and damping matrices.

Let

$$\ddot{Y} = \frac{\partial \ddot{d}}{\partial \alpha^i}, \quad \dot{Y} = \frac{\partial \dot{d}}{\partial \alpha^i} \quad \text{and} \quad Y = \frac{\partial d}{\partial \alpha^i},$$

we have

$$[M]\{\ddot{Y}\} + [C]\{\dot{Y}\} + [K]\{Y\} = -\frac{\partial [K]}{\partial \alpha^i}\{d\} - a_2 \frac{\partial [K]}{\partial \alpha^i}\{\dot{d}\}. \tag{2b}$$

Since $\{d\}$ and $\{\dot{d}\}$ have been obtained from Eq. (1), the right-hand side of Eq. (2b) can be considered as an equivalent forcing function, and the equation is of the same form as Eq. (1). Therefore, the sensitivities $\ddot{Y}$, $\dot{Y}$ and Y can also be obtained by Newmark method.

3. Inverse problem

In the forward analysis, the dynamic responses and their sensitivities with respect to a system parameter of a finite element system can be obtained from Eqs. (1) and (2). In the inverse problem, the system parameter is required to be identified from the measured responses. In other words, the parameters are chosen to best fit the experiment data. There are in general two ways to fit the data: one is simply using the least-squares method which minimizes the square error sum; the other is the sensitivity-based analysis method which has different formulation for different problems, and it is often obtained approximately by neglecting the higher order terms of the formulation. The latter approach is adopted in this study. The objective function is defined as

$$g(\alpha) = \sum_{j=1}^{l} \sum_{i=1}^{nt} \{\hat{R}_{ij} - R_{ij}\}^{\mathrm{T}} [W] \{\hat{R}_{ij} - R_{ij}\}, \tag{3}$$

where l is the number of measurement locations, nt is the number of time instances of the measured data. $\{\alpha\}$ is the vector of unknown parameters $(\alpha^1, \alpha^2, \ldots, \alpha^N)^{\mathrm{T}}$ to be identified, R is the vector of calculated response of the structure from a known set of $\{\alpha^i\}$ and $\hat{R}$ is the vector of measured response. $[W]$ is the weight matrix.

3.1. Penalty function methods

Penalty function method is generally used for modal sensitivity with a truncated Taylor series expansion in terms of the unknown parameters [26]. In this paper, the truncated series of the dynamic responses in terms of the system parameter α are used to derive the sensitivity-based formulation. The identification problem can be expressed as follows to find the vector $\{\alpha\}$ such that the calculated response best matches the measured response, i.e.

$$[Q]\{R\} = \{\hat{R}\}, \tag{4}$$

where the selection matrix $[Q]$ is a matrix with elements of zeros or ones, matching the dof corresponding to the measured response components. Vector $\{R\}$ can be obtained from Eq. (1) for a given set of $\{\alpha\}$.

Let

$$\{\delta z\} = \{\hat{R}\} - [Q]\{R\} = \{\hat{R}\} - \{R_{\mathrm{cal}}\}, \tag{5}$$

where $\{\delta z\}$ is the error vector in the measured output. In the penalty function method, we have

$$\{\delta z\} = [S]\{\delta \alpha\}, \tag{6}$$

where $\{\delta \alpha\}$ is the perturbation in the parameters, $[S]$ is the two-dimensional sensitivity matrix which is one of the matrix at time t in the three-dimensional sensitivity matrix shown in Fig. 1. For a finite element model with N elements each with M system parameters, the number of unknown parameters is $N \times M$, and $N \times M$

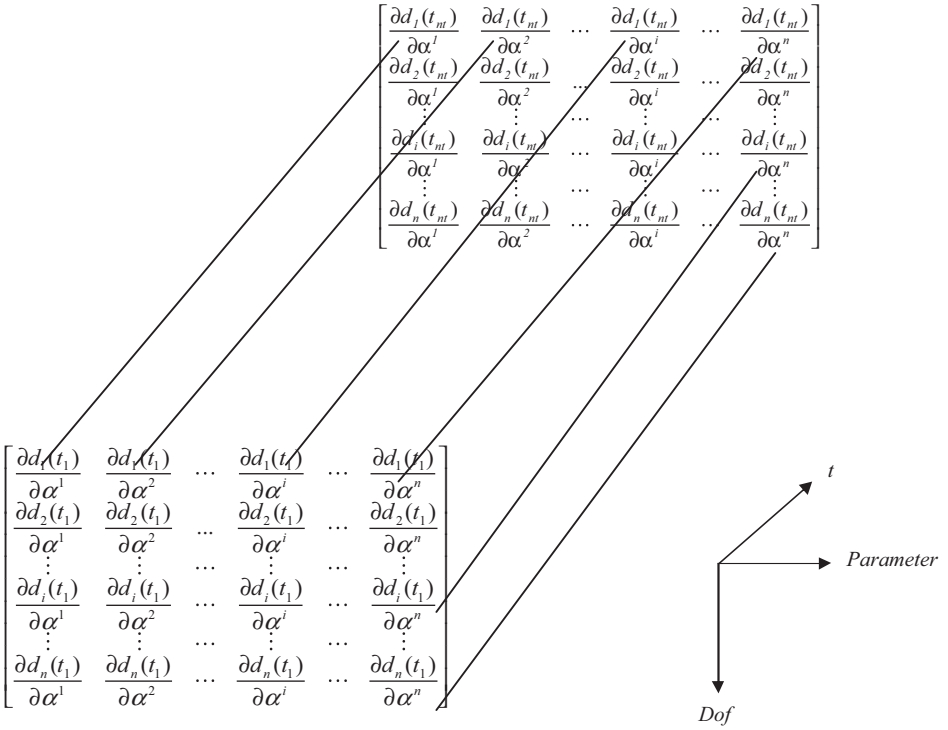

Fig. 1. Three-dimensional sensitivity matrix.

equations are needed to solve the parameters. Matrix $[S]$ is on the parameter-t plane in Fig. 1, and we can select any row of the three-dimensional sensitivity matrix, say, the ith row corresponding to the ith measurement for the purpose. When writing in full, Eq. (5) can be written as

$$\{\delta z\} = \begin{Bmatrix} \hat{R}(t_1) \\ \hat{R}(t_2) \\ \vdots \\ \hat{R}(t_l) \end{Bmatrix} - \begin{Bmatrix} R_{\text{cal}}(t_1) \\ R_{\text{cal}}(t_2) \\ \vdots \\ R_{\text{cal}}(t_l) \end{Bmatrix},$$

with $l \geqslant N \times M$ to make sure that the set of equation is over-determined. Eq. (6) can be solved by simple least-squares method as follows:

$$\delta\alpha = [S^{\mathrm{T}}S]^{-1}S^{\mathrm{T}}\delta z \tag{7}$$

or

$$\alpha_{j+1} = \alpha_j + [S_j^{\mathrm{T}}S_j]^{-1}S_j^{\mathrm{T}}(\hat{R} - R_{\text{cal}}). \tag{8}$$

The subscript j indicates the iteration number at which the sensitivity matrix is computed.

3.2. Regularization

Like many other inverse problems, Eq. (7) is an ill-conditioned problem. In order to provide bounds to the solution, the damped least-squares method (DLS) [27] is used and singular-value decomposition is used in the pseudo-inverse calculation. Eq. (7) can be written in the following form in the DLS method:

$$\delta\alpha = (S^{\mathrm{T}}S + \lambda I)^{-1}S^{\mathrm{T}}\delta z, \tag{9}$$

where λ is the non-negative damping coefficient governing the participation of least-squares error in the solution. The solution of Eq. (9) is equivalent to minimizing the function

$$J(\{\delta\alpha\},\lambda) = \|S\delta\alpha - \delta z\|^2 + \lambda\|\delta\alpha\|^2, \tag{10}$$

with the second term in Eq. (10) provides bounds to the solution. When the parameter λ approaches zero, the estimated vector $\{\delta\alpha\}$ approaches to the solution obtained from the simple least-squares method. L-curve method [28] is used in this paper to obtain the optimal regularization parameter λ.

3.3. Procedure of iteration

Usually the initial analytical model of a structure deviates from the true model and measurement from the initial intact structure is used to update the analytical model. The improved model is then treated as a reference model, and measurement from the damaged structure will be used to update the reference model. The vector of parameters found corresponds to the list of damages occurred in the structure.

When response measurement from the intact state of the structure is obtained, the sensitivities are computed from Eq. (2) based on the analytical model of the structure and the input force obtained in experiment. The vector of parameter increments is then obtained from Eq. (9) or (10) using the computed and experimentally obtained responses. The analytical model is then updated and the corresponding response and its sensitivity are again computed for the next iteration. Convergence is considered to be achieved when the criteria $||\{\alpha_{k+1}\} - \{\alpha_k\}||/||\{\alpha_{k+1}\}|| \leqslant tolerance$ is met, where $\{\alpha_k\}$ is the vector of unknown parameter calculated at the kth time instance. When measurement from the damaged state is obtained, the updated analytical model is used in the iteration in the same way as that using measurement from the intact state. The final vector of identified parameter increments corresponds to the changes occurring in between the two states of the structure. The *tolerance* is set equal to 1.0×10^{-6} in this study except otherwise specified.

Eq. (6) has been popularly used in the form of the first-order approximation of the increment on the left-hand side of the equation. The higher order term of the Taylor expansion has been omitted in the computation. The iterative computation described above on the updating of the sensitivity and the system aims at reducing error due to such omission, particularly with large local damages.

4. Computation simulation

4.1. A plane frame structure

A plane frame structure as shown in Fig. 2 is studied to illustrate the proposed method. It consists of 11 Euler–Bernoulli beam elements with 12 nodes each with three dof. The frame is fixed at nodes 1 and 12 modelled with large translational and rotational stiffnesses of 1.5×10^{10} kN/m and 1.5×10^{10} kN-m/rad, respectively. The mass density of material is 2.7×10^3 kg/m^3 and the elastic modulus of material is 69×10^9 N/m^2. The height and width of the frame are respectively 1.2 and 0.6 m, and the cross-sectional dimensions of member are $b = 0.01$ m and $h_0 = 0.02$ m with the second moment of inertia in the plane of bending equals 6.67×10^{-9} m^4. The first five undamped natural frequencies of the intact frame are 13.095, 57.308, 76.697, 152.410 and 196.485 Hz. Rayleigh damping model is adopted with the damping ratios of the first two modes taken equal to 0.01. The equivalent Rayleigh coefficients a_1 and a_2 are respectively 1.3395 and 4.52×10^{-5}.

4.1.1. Features of the response sensitivities

The time response depends on the excitation force, and the sensitivity of the response with respect to perturbation of a local system parameter would be different. This study is to find what type of force excitation would be best for damage detection using the proposed method. Sinusoidal, impulsive and random excitations are studied to calculate the dynamic responses and their sensitivities with respect to a system parameter of the frame. The elastic modulus of material in element 1 is selected as the perturbed parameter.

The excitation force is applied at node *2* along the x-direction. The sinusoidal force is taken as $F(t) = 10\sin(2\pi ft)$ N where f is the excitation frequency taken equal to the first and third modal frequencies of the frame and at 25 Hz, which is between the first and second modal frequencies. The impulsive force lasting for

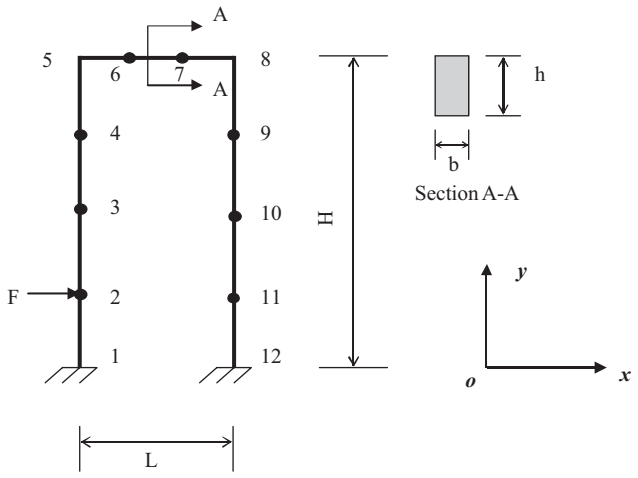

Fig. 2. The plane frame structure.

0.1 s duration is expressed in the following form with a magnitude of 10 N:

$$F(t) = \begin{cases} 200(t - 0.05), & 0.05 \leqslant t \leqslant 0.1, \\ 200(0.15 - t), & 0.1 \leqslant t \leqslant 0.15. \end{cases}$$

Uniformly distributed random force between $+10$ and -10 N and normally distributed random force between 0 and 10 N are also applied separately.

The response is measured along the x-direction at node 9 with a sampling rate of 500 Hz including the first five modes of the structure.

Figs. 3–8 show the time histories of the excitation force, the displacement response and its sensitivity, plus the acceleration response sensitivity with respect to the perturbed system parameter for each type of the forces described above. Since the magnitudes of all the excitation forces are equal, a direct comparison of the responses and their sensitivities is possible.

Fig. 3 gives the sensitivities from sinusoidal excitation at the undamped fundamental frequency of the structure. The amplitude of the displacement response increases gradually until the energy input is balanced by the energy dissipated from damping where the amplitude becomes relatively stable. In the computation of the sensitivities from Eq. (2), the forcing function consists of both the displacement response and the velocity response. The velocity is approximately one thousand times larger than the displacement. However the second term on the right-hand-side of the equation is one hundred times smaller than the first term because of the small damping coefficient a_2. Therefore the forcing term in Eq. (2) is dominated by the displacement response which increases in the first stage and becomes relatively constant later. Therefore, the amplitude of the sensitivities obtained also increases with time and it becomes stable when the energy input and energy dissipation are balanced.

Fig. 4 gives the sensitivities from sinusoidal excitation at the third undamped natural frequency of the structure. Explanation on the pattern of the curves is similar to Fig. 3. The small variation in the amplitudes of the response and the sensitivities in Fig. 4 have been checked with Fast Fourier Transform (FFT) analysis. The irregular waveform in the first 5 s is due to the transient responses from the first few modes arising from the application of the excitation. The response after 20 s is dominated by a component at the excitation frequency as shown in the FFT spectrum in Fig. 9.

Fig. 5 gives the sensitivities from sinusoidal excitation at 25 Hz, which is between the first and the second natural frequencies of the structure. The displacement response consists of a combination of responses mainly at the first and second natural frequencies of the structure. This can be explained by the modal superposition principle. This response becomes relatively stable with time under the damping effect. The sensitivities obtained under the forcing function dominated by the displacement response also consist of components at

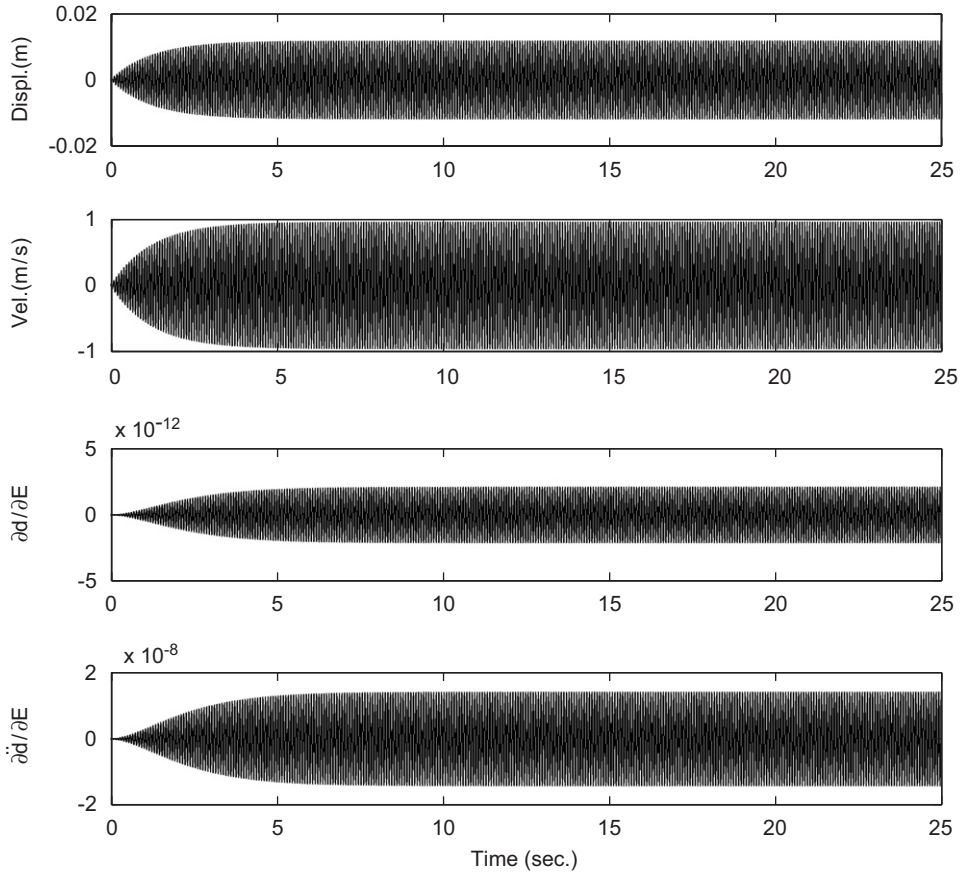

Fig. 3. Responses and response sensitivities when under sinusoidal excitation at the undamped fundamental frequency.

both frequencies but with the component at the first natural frequency dominating. The sensitivities diminish with time but maintain a small amplitude of vibration because of the relatively stable input dominated by the displacement response.

Fig. 6 gives the response sensitivities from impulsive excitation. The displacement response is dominated by the first natural frequency of the structure with the higher frequency components diminish rapidly with damping. The response reduces to zero with time. The sensitivities obtained from Eq. (2) increase with the input energy larger than the dissipated energy and reach a maximum at around 1.2 s. All the sensitivities diminish to zero with time under the damping effect.

Fig. 7 gives the response sensitivities from uniformly distributed random excitation. The first five modes of the structure are excited with strong contribution to the displacement response. The sensitivities obtained from Eq. (2) are under the force excitation dominated by the displacement response with vibration at the first five natural frequencies of the structure, and they also consist of a combination of components at the first five natural frequencies of the structure with both increasing and decreasing amplitude under the damping effect. The sensitivities will not diminish to zero with time as the displacement responses always exist under the random excitation.

Fig. 8 gives the response sensitivities from normally distributed random excitation. Observations with the responses and their sensitivities are similar to those obtained from under uniformly distributed random excitation.

The shapes of the three types of response sensitivities in time are similar for each type of excitation, but it is different for different excitation. A comparison of the sensitivities in Figs. 3–8 shows that sinusoidal excitation would give higher sensitivities than random force excitations while those from impulsive excitation exhibit the smallest sensitivity. This may be due to the reason that there is only one impact acting on the frame in the

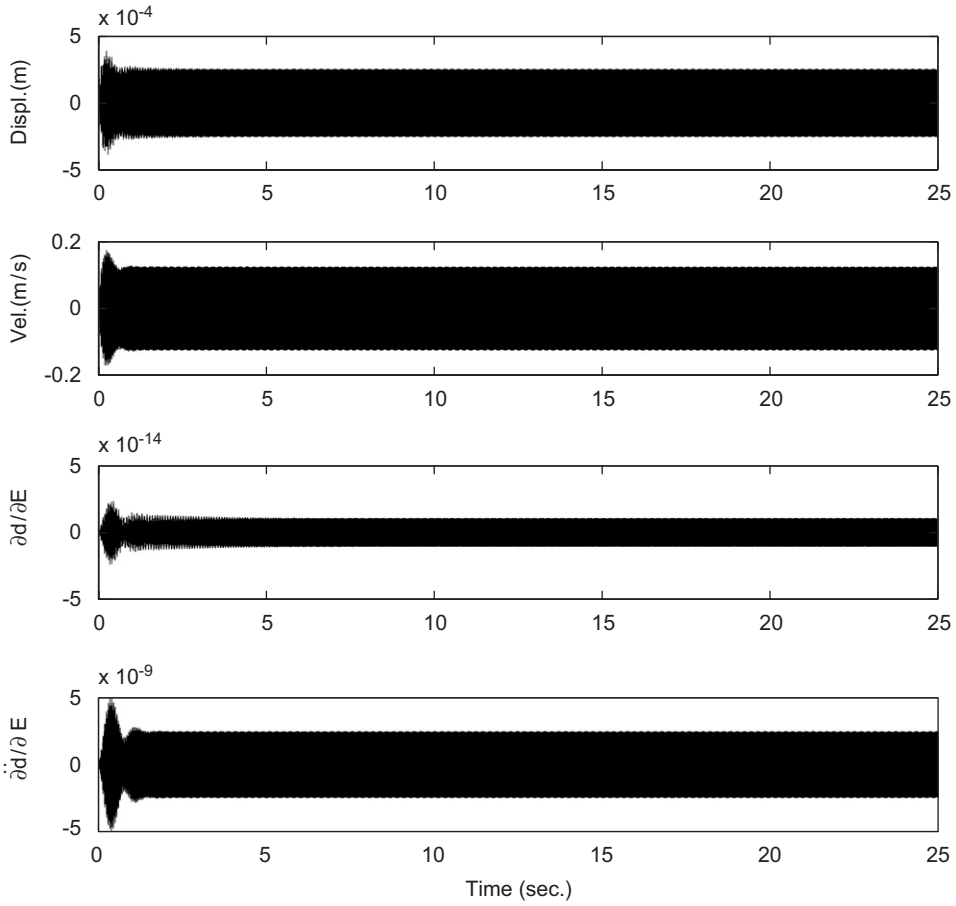

Fig. 4. Responses and response sensitivities when under sinsuodal excitation at the third undamped natural frequency.

duration studied, while the other excitations act on the frame continuously in the same period giving higher energy input. The sensitivities from excitation at lower modal frequency of the structures are larger than those from a higher modal frequency. But the sensitivities from excitation at a lower frequency which is not a modal frequency are very small. These observations show that the sensitivities are dependent on the displacement response of the structure as seen in Eq. (2). This can be further explained from the view point of energy input: the largest energy input on the structure is from the sinusoidal excitation at the first natural frequency, such that the sensitivities are largest under this excitation. The smallest energy input is from the impulsive force and the sensitivities are the smallest.

4.1.2. Damage scenarios

Six damage scenarios of single and multiple damages in the frame with and without measurement noise are studied and they are shown in Table 1. Three more scenarios with different types of model errors are also included as Scenarios 7–9. Local damage is simulated with a reduction in the elastic modulus of material of an element. Sinusoidal excitation of $F = 10\sin(12\pi t)$ N is used for the identification with a frequency well below the fundamental frequency of the structure. The sampling rate is 1000 Hz and 200 data of the response collected along the x-direction at node 9 are used in the identification unless otherwise specified. The relative percentage error in the identified result is defined as

$$\text{Relative error } (\%) = \frac{||\{\alpha_{id}\} - \{\alpha_{\text{true}}\}||}{||\{\alpha_{\text{true}}\}||} \times 100\%,$$

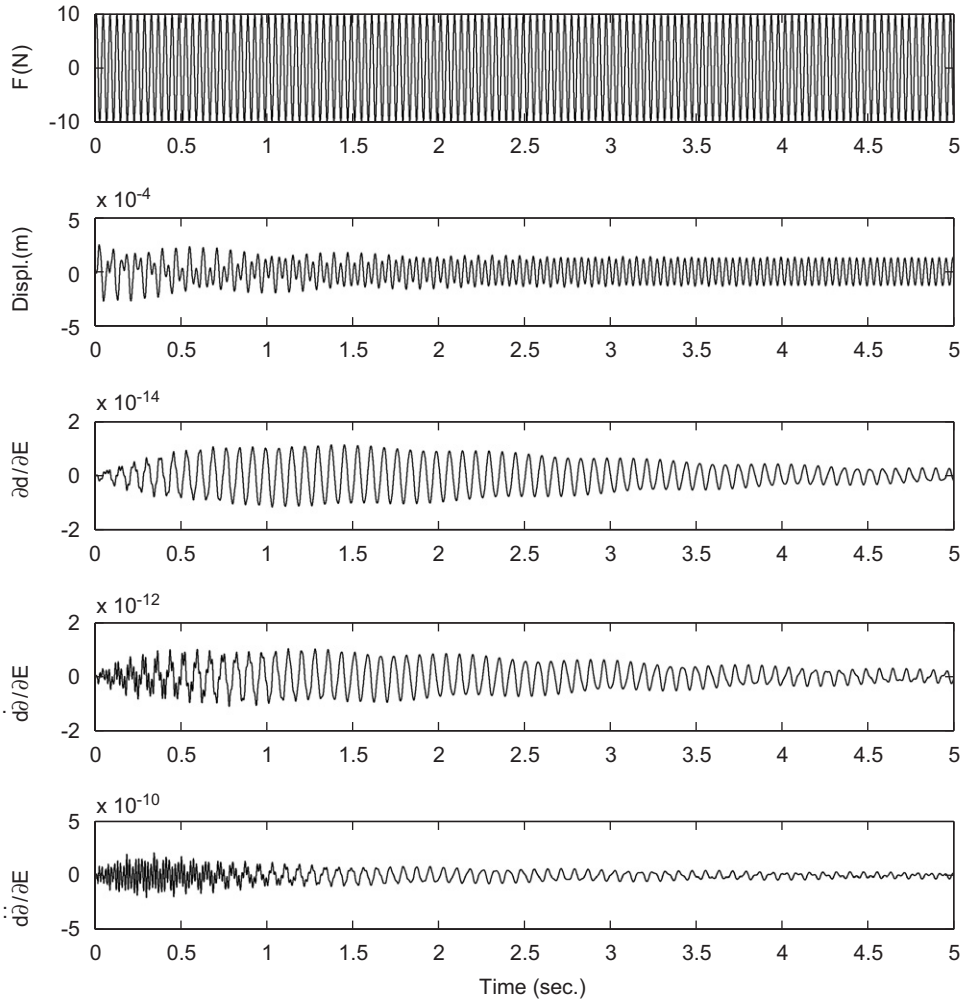

Fig. 5. Response sensitivity from sinusoidal excitation at 25 Hz.

where $\{\alpha_{id}\}$ and $\{\alpha_{\text{true}}\}$ are vectors of the identified and true values of the parameter, respectively. The damage locations can be identified correctly in all the Scenarios, and the relative error is shown in Table 2.

Scenarios 1 and 2 study the single damage scenarios with different excitation frequency. The sinusoidal excitation described above at 6 and at 25 Hz are used for the two scenarios, respectively. The displacement response along the x-direction at node 9 is used for the identification. The iterative solution converges after 13 and 15 iterations respectively with a maximum error of 0.1% and 0.01% in element 5 for the two scenarios respectively, and the corresponding optimal regularization parameters are 8.6×10^{-15} and 8.7×10^{-15} respectively. The excitation frequency seems not to have significant effect on the identified results.

Scenarios 3–5 are on multiple damages with different type and amount of measured responses for the identification. Damages in the frame are modeled with 5% reduction in the elastic modulus of material in both elements 3 and 6. The sinusoidal excitation force at 6 Hz and measured displacement as for Scenario 1 is used for Scenario 3, while acceleration response at the same dof is used for Scenario 4 and two displacement responses in the global x-direction at node 9 and in the global y-direction at node 5 are used for Scenario 5. Very good results are obtained after 22, 16 and 21 iterations respectively, and Table 2 gives the error of identification in all the elements with a maximum error of −0.36% in element 9, 0.12% in element 5 and −0.20% in element 9 for the three scenarios respectively. The optimal regularization parameter is 6.8×10^{-15}, 2.9×10^{-10} and 1.5×10^{-15} respectively. Acceleration response is noted to give better identified results then

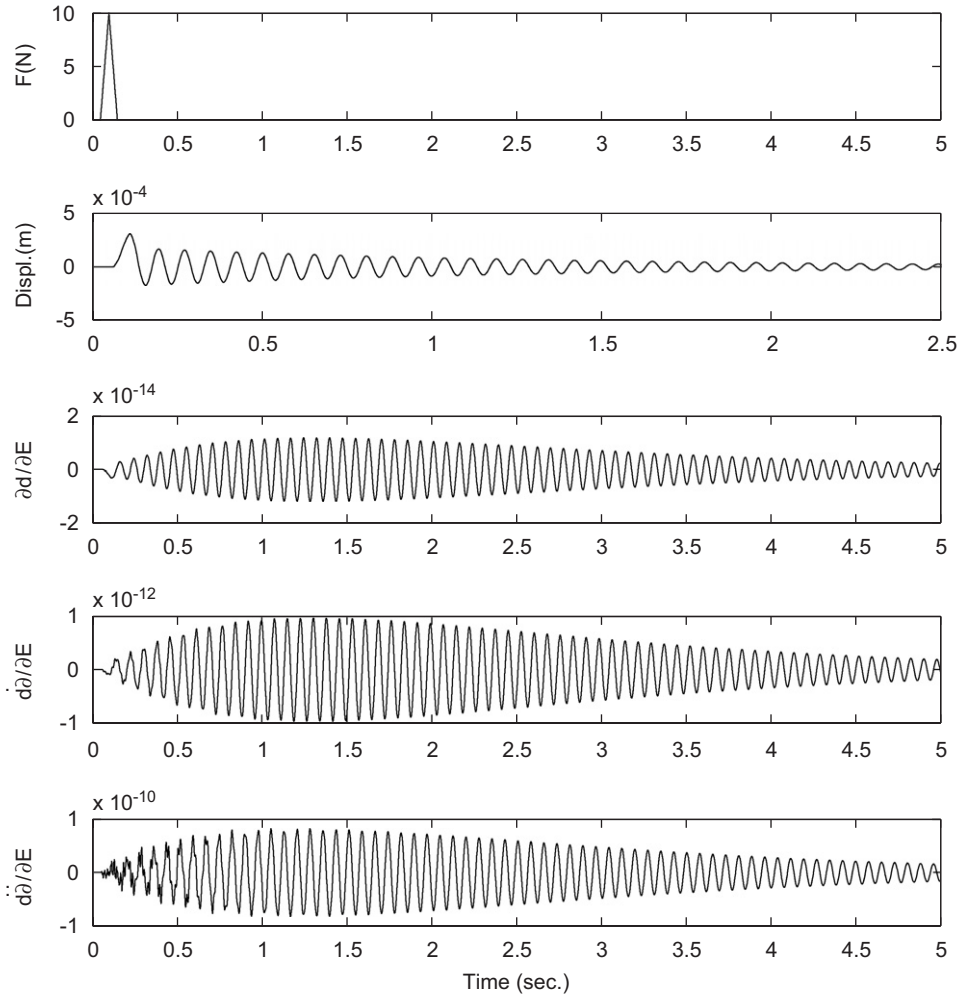

Fig. 6. Response sensitivity from impulsive excitation.

displacement response, while the relative identified error is reduced by about 50% when more displacement data is used in the identification (Scenario 3 versus Scenario 5). Fig. 10 compares the "measured" displacement and acceleration responses of the structure with damage Scenario 2, the calculated responses of the initial structure and the reconstructed responses from the final updated structure. The local damage is small and its effect on the global dynamic response is very small as shown in the figure. The "measured" and reconstructed responses are, however, observed to be very close to each other.

Scenario 6 studies the effect of measurement noise on the identification. A normally distributed random error with zero mean and a unit standard deviation is added to the measured displacement as

$$\hat{d} = d_{\text{cal}} + E_p N_{\text{oise}} \operatorname{var}(d_{\text{cal}}),$$

where $\hat{d}$ is the vectors of polluted displacement; E_p is the noise level; N_{oise} is a standard normal distribution vector with zero mean and unit standard deviation; $\operatorname{var}(\cdot)$ is the variance of the time history; d_{cal} is the vector of calculated displacement. Scenario 1 is again studied. The two displacement responses as for last study are used for the identification with 10% noise included. Satisfactory results are obtained after 41 iterations with a maximum error of 2.5% in element 6. The optimal regularization parameter is 6.3×10^{-14}. The convergence tolerance has been increased to 5.0×10^{-7} allowing larger variation in the iteration results. Higher relative

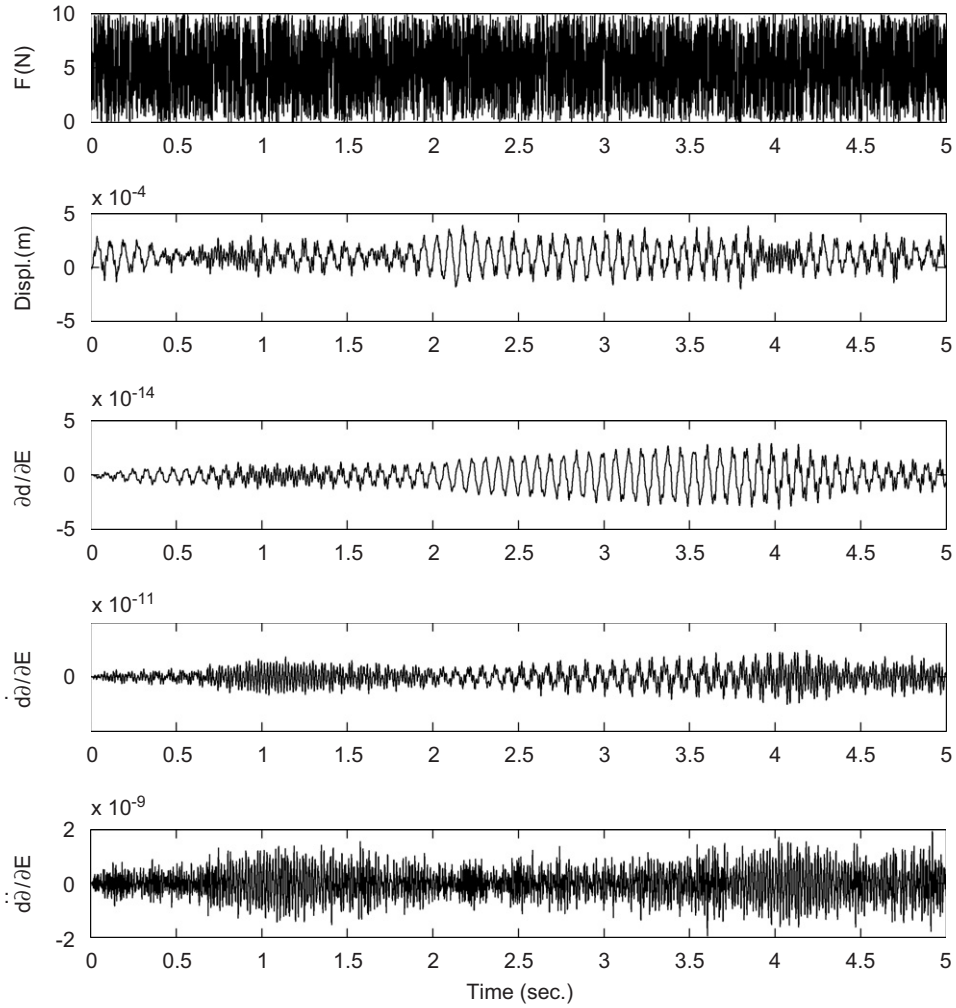

Fig. 7. Response sensitivity from uniformly distributed random excitation.

errors are found in the identified results when comparing with the noise-free results indicating that measurement noise has large effect on the damage identification.

Scenarios 7–9 are on the effect of different types of initial model error to the identification. Scenario 7 consists of no simulated damage in the structure, but with the initial elastic modulus of material of all the elements under-estimated by 5% in the inverse identification. The simulated ''measured'' responses as for last scenario are computed using the true elastic modulus of material with additional 10% random noise. The solution converges to the true value in 286 iteration steps with a maximum error of −2.65% in element 5 with an optimal regularization parameter of 8.3×10^{-15}. This study illustrates the accuracy of the proposed approach with a practical system updating with model error. A relatively good finite element model is therefore needed for the presented damage detection.

Scenario 8 restudies Scenario 7 but with the first two modal damping ratio change from 0.01 to 0.02 in the inverse identification. The same ''measured'' responses calculated with the true parameters as for Scenario 6 are used for the identification. The identification results converge to the true value after 42 iterations with a maximum error of 2.69% in element 6 and with an optimal regularization parameter of 6.4×10^{-14}.

Scenario 9 restudies Scenario 7 but with changes in the support stiffnesses. The support stiffnesses in the finite element model are reduced to 1/10th of the original values in the inverse identification. The identification

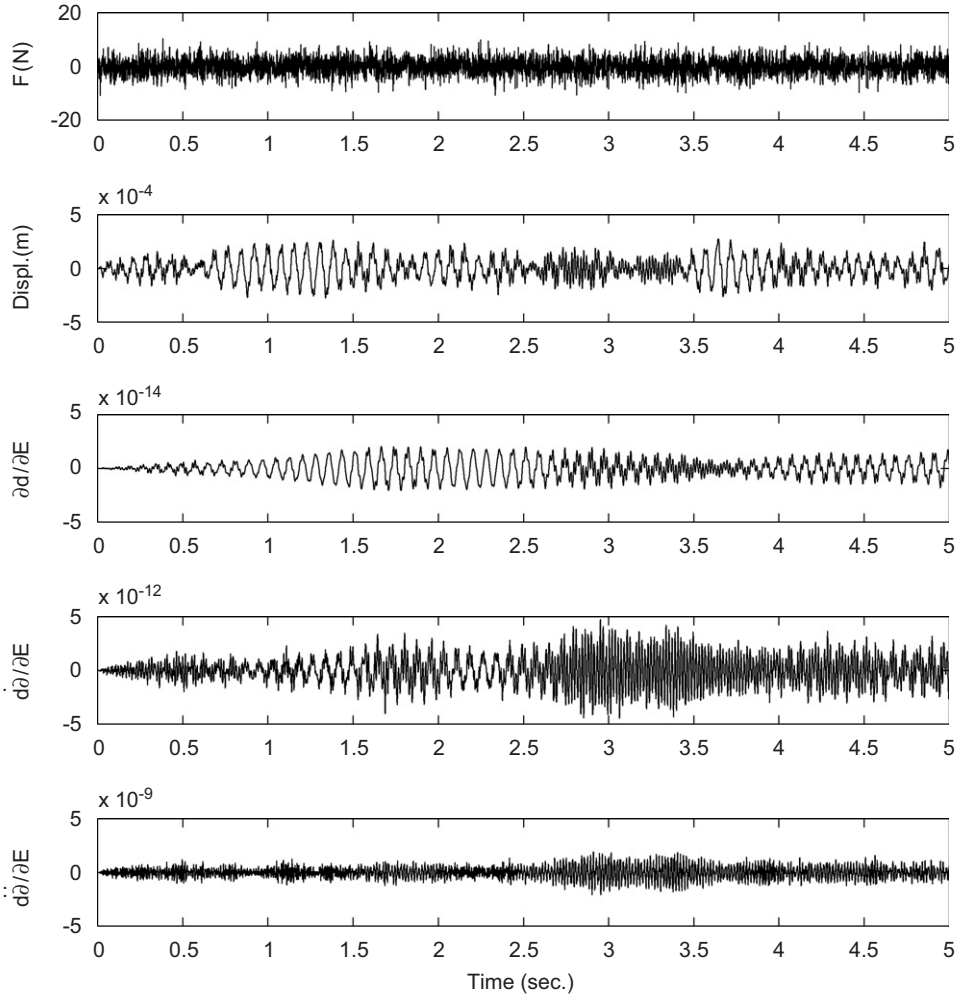

Fig. 8. Response sensitivity from normally distributed random excitation.

results converge to the true value after 45 iterations with a maximum error of 2.54% in element 6 and with an optimal regularization parameter of 6.5×10^{-14}. Result from Scenarios 7–9 shows that the proposed approach of system identification is less affected by initial model errors.

4.2. The European Space Agency Structure

The European Space Agency Structure (ESAS) is studied as another numerical example to illustrate the effectiveness of the proposed method. The finite element model of the structure is shown in Fig. 11. The structure is modeled by 48 frame elements and 44 nodes with three dofs at each node for the translation and rotational deformations. Each frame element is constructed by integrating an Euler-Bernoulli beam element with a rod element. The modulus of elasticity of material is $7.5 \times 10^{10}\,\mathrm{N/m^2}$ and the density is $2800\,\mathrm{kg/m^3}$. The total number of dofs in the analytical finite element model is 132. The first twelve natural frequencies of the intact ESAS structure are 16.86, 63.13, 80.05, 131.34, 173.33, 196.23, 201.73, 214.42, 221.81, 246.60, 274.68 and 284.13 Hz. Rayleigh damping is used for constructing the damping matrix, and the modal damping ratios of the first two modes are taken as 0.01 and 0.02 respectively.

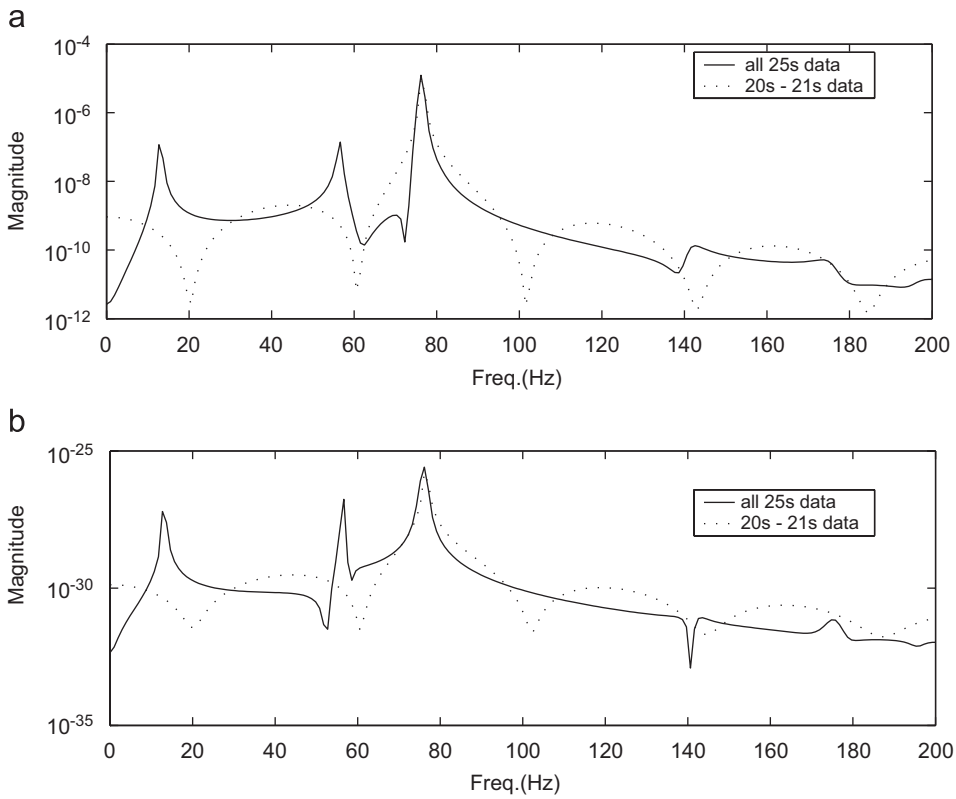

Fig. 9. FFT spectrum for the displacement response and its response sensitivity ((a) displacement; (b) displacement response sensitivity).

Table 1
Damage Scenarios for plane frame structure

Damage scenario	Damage location (element no.)	Reduction in elastic modulus	Noise	Measurement
1	6	5%	Nil	9*x*-displacement
2	6	5%	Nil	9*x*-displacement
3	3 and 6	5%, 5%	Nil	9*x*-displacement
4	3 and 6	5%, 5%	Nil	9*x*-acceleration
5	3 and 6	5%, 5%	Nil	9*x*, 5*y*-displacement
6	6	5%	10%	9*x*, 5*y*-displacement
7	No damage	5% under-estimation in the elastic modulus of all elements	10%	9*x*, 5*y*-displacement
8	6	5% reduction + increase of damping ratios from 0.01 to 0.02	10%	9*x*, 5*y*-displacement
9	6	5% reduction + support stiffnesses reduced to 1/10th of their original values	10%	9*x*, 5*y*-displacement

4.2.1. Damage detection studies

Damage in the structure is simulated as a reduction in the stiffness of individual element, represented as a reduction in the elastic modulus of material, with the other properties remain unchanged. Four damage scenarios are studied as listed in Table 3. A sinusoidal excitation force of $F = 5000\sin(22\pi t)$ N is applied at the end of the cantilever structure along the global negative y-direction as shown in Fig. 11.

Table 2
Error (%) in the identified results of damage Scenarios 1–9

Damage scenarios	Noise	Error (%) in each element										
		1	2	3	4	5	6	7	8	9	10	11
1	—	0.0	0.0	0.0	0.0	0.1[a]	0.0	0.0	0.0	0.0	0.0	0.0
2	—	0.0	0.0	0.0	0.0	0.01[a]	0.0	0.0	0.0	0.12	0.0	0.0
3	—	−0.04	−0.08	0.24	−0.31	0.26	−0.02	0.12	0.25	−0.36[a]	0.13	−0.02
4	—	0.01	−0.02	−0.03	0.01	0.12[a]	−0.01	−0.12	0.01	0.03	0.02	−0.02
5	—	−0.02	−0.04	0.12	−0.16	0.13	−0.01	0.06	0.12	−0.20[a]	0.06	−0.01
6	10%	0.93	1.32	−0.82	1.18	−0.96	2.50[a]	−1.91	1.11	0.85	1.43	−1.05
7	10%	0.13	−0.48	−0.3	0.31	−2.65[a]	0.18	−0.79	-0.5	−0.9	0.79	0.86
8	10%	1.16	1.42	−0.86	1.23	−1.02	2.69[a]	−1.96	1.14	0.96	1.52	−1.26
9	10%	0.95	1.34	−0.81	1.16	−0.98	2.54[a]	−1.93	1.13	0.86	1.42	−1.08

[a]Denote the largest value in the group.

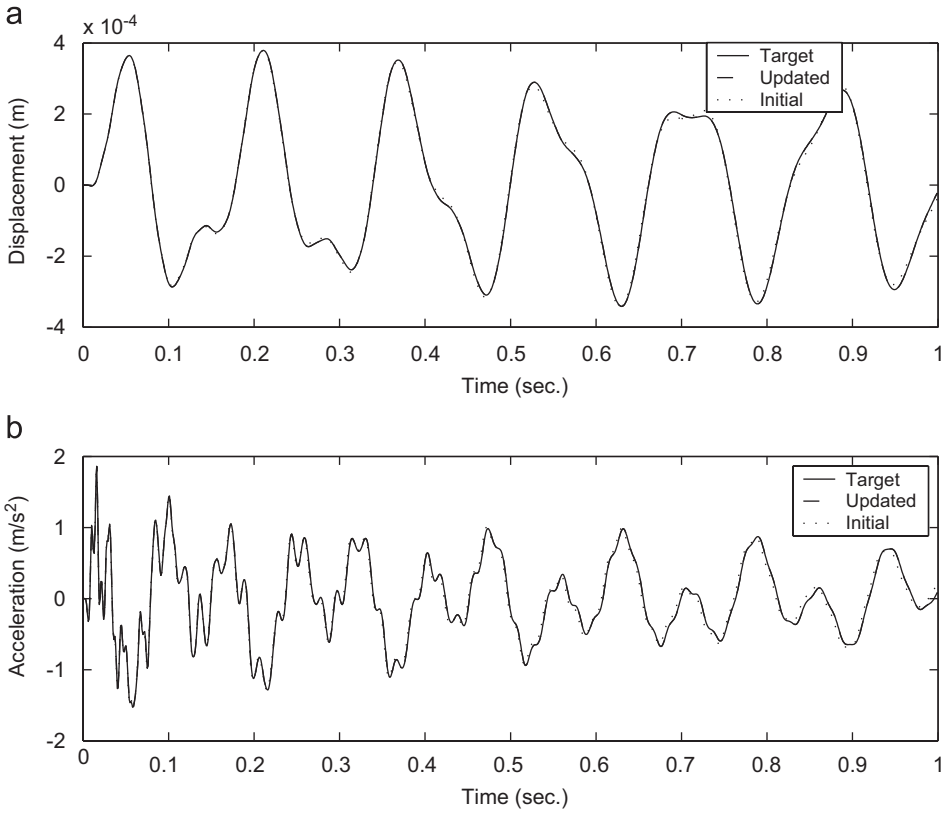

Fig. 10. Comparison of the ''measured'' dynamic responses of the structure with Scenario 2 and the responses of the initial structure and reconstructed responses of the updated structure.

4.2.1.1. Scenario 10: study on multiple damages close to the supports. Two local damages are introduced in elements 1 and 13, which are adjacent to the supports of the structure. The sampling rate is 500 Hz and one second of ''measured'' data is used for the identification. The local damages are identified after 25 steps of iteration with the optimal regularization parameter equals to 1.2×10^{-10}. Fig. 12 shows that the two local

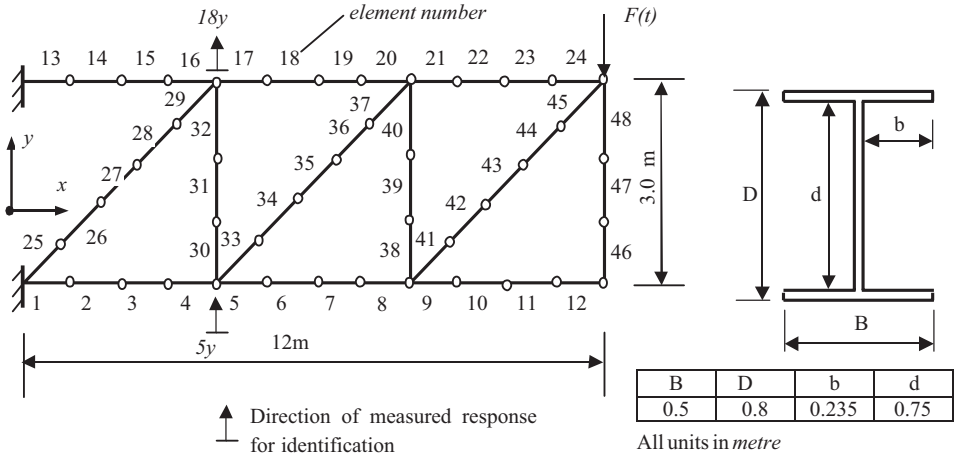

Fig. 11. Finite element model of the European Space Agency Structure.

Table 3
Damage scenarios for ESAS structure studies

Damage scenarios	Damage location (element no.)	Reduction in elastic modulus	Noise	Measurement
10	1 and 13	10%	Nil	*5y*-acceleration
11	20, 21, 35, 36, 37, and 40	10%, 7%, 15%, 10%, 10% and 10%	Nil	*5y* and *18y*-acceleration
12	1, 13, 20, 21, 35, 36, 37, and 40	10%, 10%, 10%, 7%, 15%, 10%, 10% and 10%	Nil	*5y* and *18y*-acceleration
13	1, 13, 20, 21, 35, 36, 37, and 40	10%, 10%, 10%, 7%, 15%, 10%, 10% and 10%	1%, 10%	*5y* and *18y*-acceleration

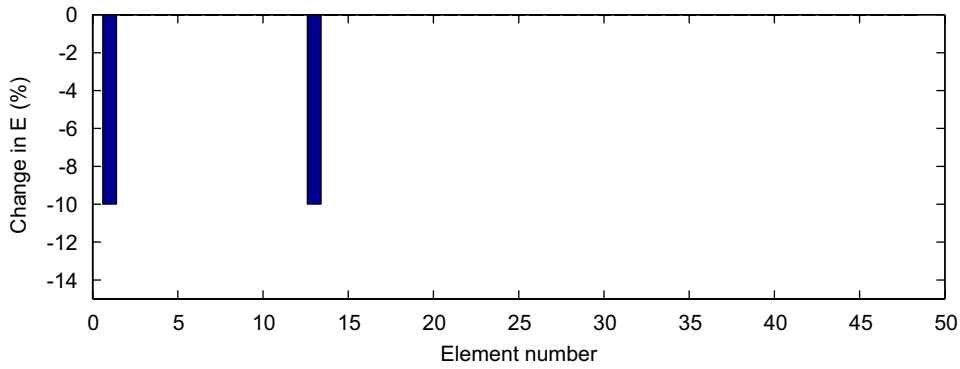

Fig. 12. Identification of multiple damages near the supports.

damages are identified very accurately with a maximum relative error less than 0.1%, while there is no error in all other elements. This shows the efficiency and the accuracy of the proposed method.

4.2.1.2. Scenario 11: study on the effect of different sampling rate. Six local damages are introduced in elements 20, 21, 35, 36, 37 and 40. These damages are adjacent to each other as shown in Fig. 11, simulating a

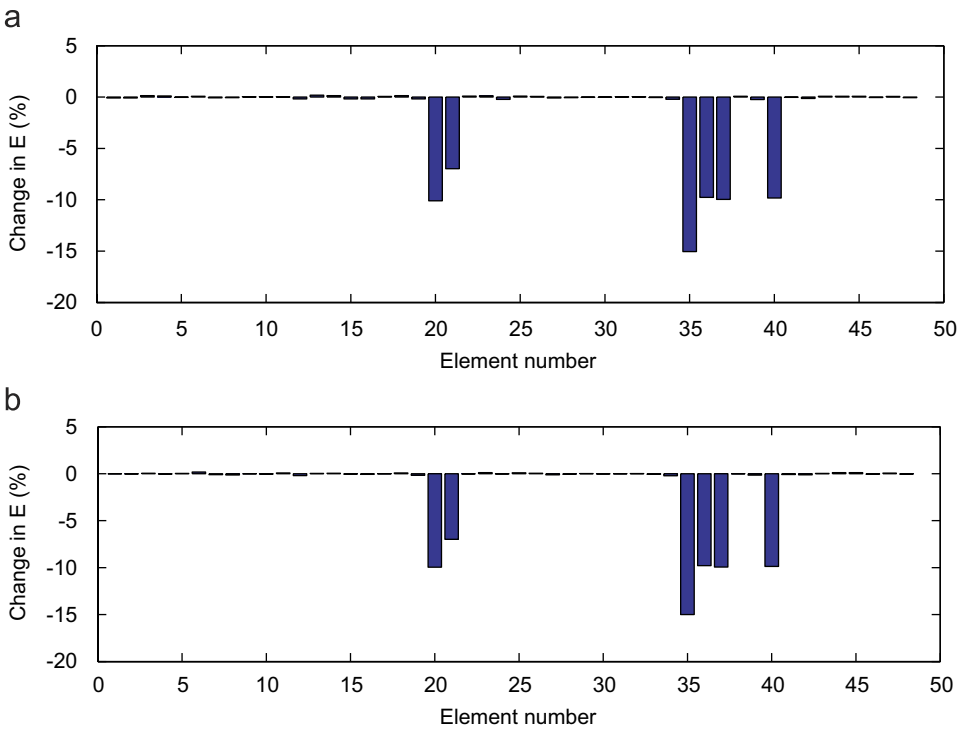

Fig. 13. Identified damages from different sampling rates: (a) sampling rate = 500 Hz; and (b) sampling rate = 200 Hz.

damage zone spanning over several members of the structure through a joint connection. Two sampling rates are studied: (a) 500 Hz, which includes the first 10 modes of the structure; (b) 200 Hz, which includes the first 3 modes. One second of the "measured" acceleration responses from the 5th node along the global y-direction and the 18th node along the global y-direction are used in the identification. The required iteration numbers are 26 and 29 for the cases of 500 and 200 Hz sampling rates respectively and the optimal regularization parameters are found to be 1.24×10^{-10} and 1.31×10^{-10} respectively. Fig. 13 indicates that the local damages are identified very accurately with no alarm in other elements. This shows that a sampling rate as low as 200 Hz can give good accuracy in the identified results.

4.2.1.3. Scenario 12: Effect of amount of measured data for identification. The group of damages in Scenario 11 is enlarged to include two more local damages in elements 1 and 13. Two different lengths of data are studied: (a) 200 data points; and (b) 500 data points. The same acceleration responses for the last study are used. The sampling rate is 500 Hz. The required iteration numbers are 27 and 30 for Cases (a) and (b) respectively and the regularization parameters are 1.26×10^{-10} and 1.34×10^{-10} respectively. Fig. 14 shows that the local damages are identified very accurately with no alarm in other elements. This shows that data length as short as 200 is sufficient to give good accuracy of the identified results so long it is larger than the number of unknowns.

4.2.1.4. Scenario 13: Effect of measurement noise. The last damage scenario is re-examined with a sampling rate of 500 Hz and the same set of "measured" acceleration response as for last study is used. 1% and 10% noise level are separately included in the measured response data. The required iteration numbers are 31 and 35 for the cases with 1% and 10% noise level respectively and the optimal regularization parameters are found to be 1.36×10^{-10} and 1.41×10^{-10} respectively. Fig. 15 shows that the measurement noise has large effect on the identified results in comparison with the noise free studies above. The maximum relative error for 1% noise level is -3% in element 20 and for 10% noise level is 5.1% in element 13 while there are false alarms in

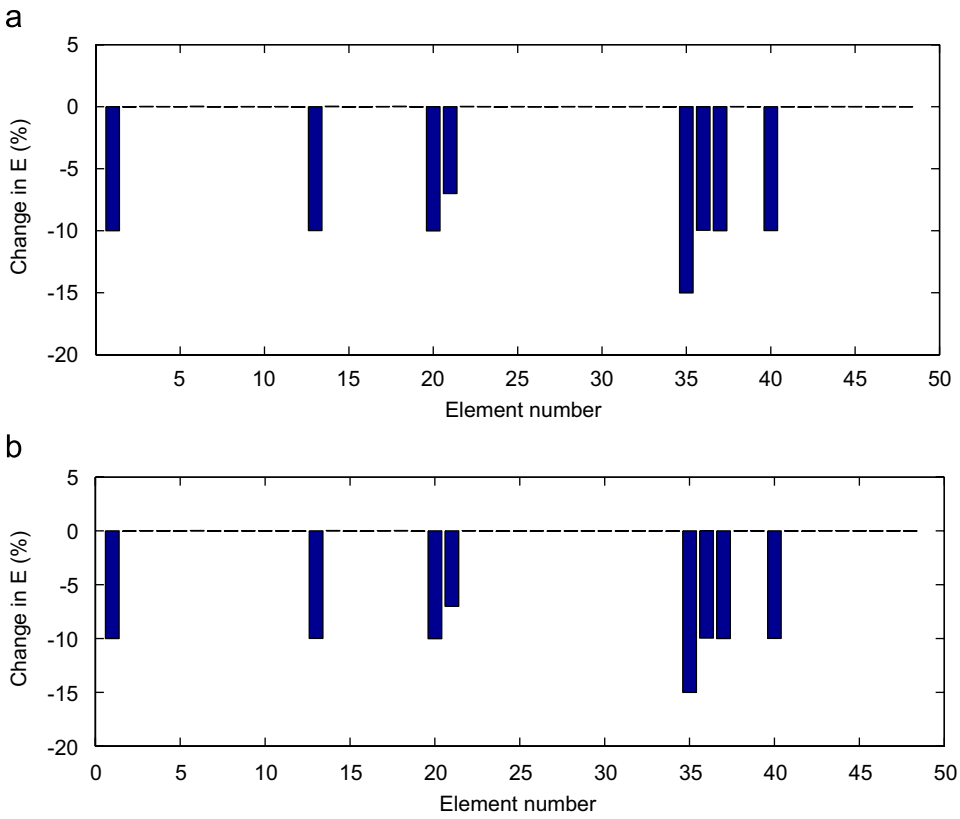

Fig. 14. Identified damages from different data points: (a) data points = 200; and (b) data points = 500.

elements 12 and 24. These results indicate that the measured noisy data is preferably to be improved before it is used for damage detection in real application.

5. Experimental verification

5.1. Free–free supported steel beam

Two simple structures have been tested in the laboratory to verify the proposed method. The first experiment is with a free–free supported steel beam. The length, width and height of the beam are respectively 2.1, 0.025 and 0.019 m, and the elastic modulus and mass density of the material are $2.07 \times 10^{11}\,\mathrm{N/m^3}$ and $7.83 \times 10^{3}\,\mathrm{kg/m^3}$ respectively. The beam is suspended at its two ends as shown in Fig. 16. It is discretized into 20 Euler–Bernoulli beam elements with three dof at each node. The flexural rigidity of all the elements is taken as the unknowns to be identified in the inverse analysis. The first five natural frequencies of the intact beam are 22.87, 62.76, 123.05, 203.24 and 303.45 Hz from modal test of the beam. A sinusoidal force at the frequency of half of the first natural frequency of the beam was applied at the nodal point of the first vibration mode of the beam 480 mm from the left free end with an exciter model Ling Dynamic LDS V450. The lateral acceleration obtained with a B&K 4370 accelerometer at the middle of the beam was used to identify these unknown flexural rigidities. Sampling frequency is 2000 Hz. Time history of the input sinusoidal force was also recorded for calculating the numerical response of the beam. The acceleration response data of the first five seconds is used for the damage detection. Rayleigh damping is adopted and the modal damping ratios were recorded as 0.007 and 0.01 for the first two modes from the dynamic response. With experiences from the numerical study above, the high frequency measurement noise in the measured acceleration was removed using 21-point

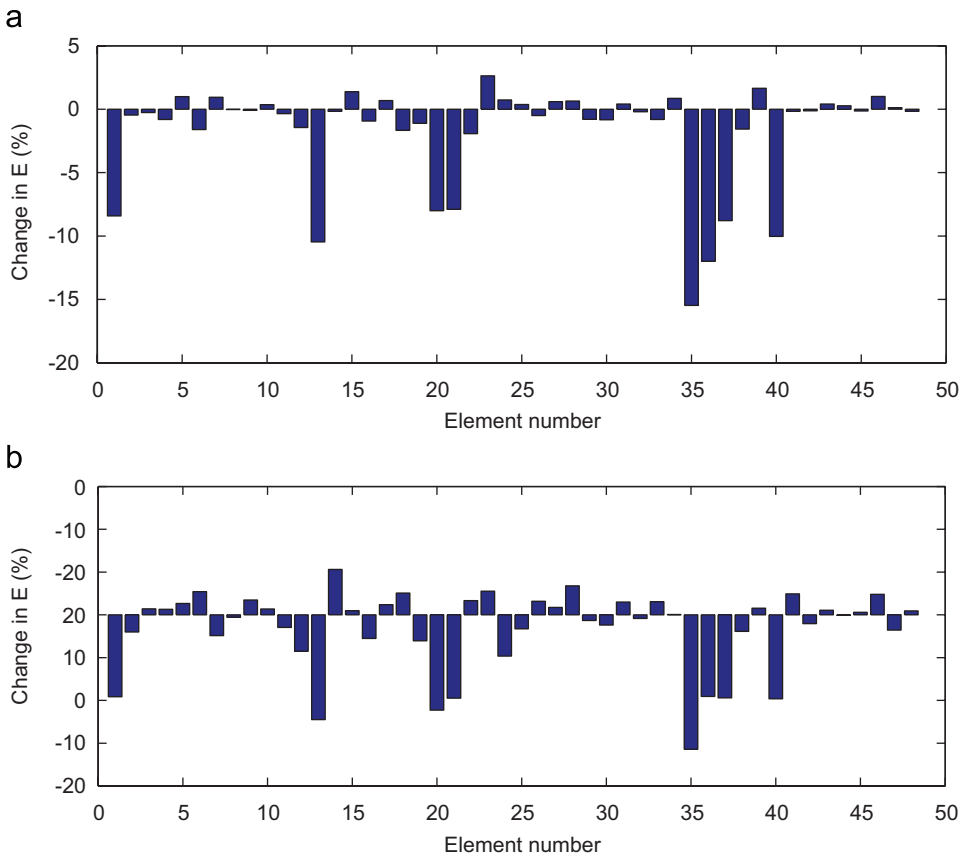

Fig. 15. Identified damages from under different noise levels: (a) noise level = 1%; and (b) noise level = 10%.

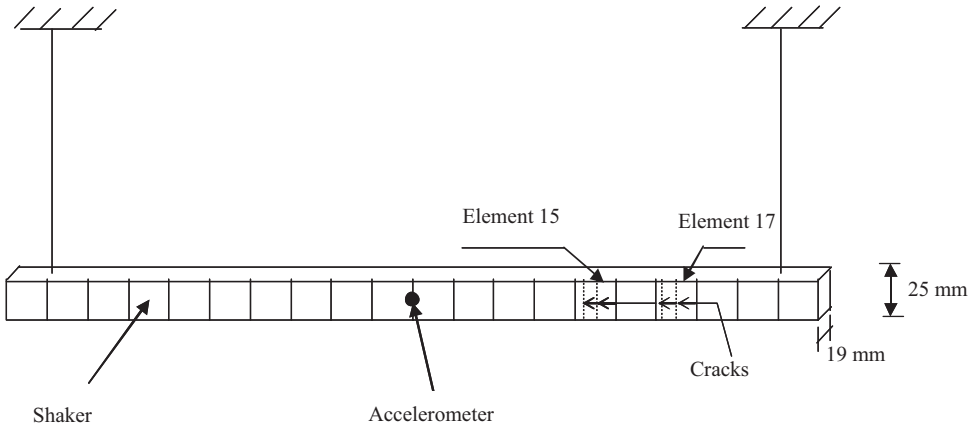

Fig. 16. Configuration of free–free steel beam for force vibration test.

moving average. The convergence tolerance in the iteration is changed to 5.0×10^{-7} allowing for larger variation in the iterative results.

It is known that the finite element modeling error in the intact structure has, in general, significant effect on the accuracy of the damage identified results. In most cases, the initial finite element is updated first to obtain a good representation of the intact structure. Table 4 lists the first five frequencies of the intact beam from

Table 4
The measured and the analytical natural frequencies (Hz) and the relative error (%) of the steel free-free beam with multiple cracks

Crack scenarios	Mode				
	1	2	3	4	5
No crack					
Experimental	22.87	62.76	123.05	203.24	303.45
Analytical	22.83/−0.18	62.74/−0.03	123.04/−0.0	203.03/−0.12	302.86/−0.2
Two cracks					
Experimental	22.74	61.77	119.75	198.49	299.50
Analytical	22.71/−0.22	62.25/−0.03	120.73/0.82	200.55/1.04	301.37/0.62
Four cracks					
Experimental	21.97	56.58	110.96	188.38	289.87
Analytical	21.96/0.0	56.94/0.64	111.82/0.78	190.01/0.87	288.33/−0.53

Note: $\cdot/\cdot$ denotes the modal frequency/relative error.

eigenvalue analysis as well as the experimental frequencies. It is noted that these two sets of frequencies match each other very well indicating the finite element model of the beam is good enough for damage detection. Two damage scenarios were then created for the study.

5.1.1. Scenario E1: Single damage element

Two cracks are introduced at 1.66 and 1.72 m from the left free end with 3 and 9 mm crack depth respectively, and they are created using a machine saw with 1.3 mm thick cutting blade. The two cracks are close to each other and both of them are in element 17 of the finite element model. The crack damage is modeled as a reduction in the flexural rigidity of this element. The first five measured natural frequencies of the damaged beam are 22.74, 61.77, 119.75, 198.49 and 299.5 Hz respectively. The equivalent damage is calculated as 12.8% reduction in the flexural rigidity of the cracked element with a crack model [29], such that the first five calculated modal frequencies are: 22.71, 62.25, 120.73, 200.55 and 301.37 Hz matching closely with the experimental modal frequencies with very small relative errors as shown in Table 4. Very good prediction on the damage in element 17 is obtained after 77 iterations as shown in Fig. 17(a), and the errors in the identified results are shown in Table 5 with a maximum error of −2.43% in element 18 adjacent to the damage element. The optimal regularization parameter is 6.7×10^{-9}.

5.1.2. Scenario E2: Multiple damage elements

The two cracks in the last Scenario are deepened to 12 mm each. Another two cracks are introduced at 1.49 and 1.52 m from the left free end of the beam with 9 and 6 mm depth respectively. Both the latter two cracks are in element 15. The first five experimental natural frequencies of the damaged beam are 21.97, 56.58, 110.96, 189.33 and 289.06 Hz. The equivalent damages for the two sets of cracks are calculated as 37.4% and 57.6% reduction in the flexural rigidity of elements 15 and 17 respectively, such that the first five calculated modal frequencies are: 21.96, 56.94, 111.82, 190.01 and 288.33 Hz matching closely with the experimental modal frequencies with very small relative errors as shown in Table 4.

Good identified results are obtained after 95 iterations as shown in Fig. 17(b). The errors in the identified results are shown in Table 5 with a maximum error of −4.34% at element 17. The corresponding optimal regularization parameter is 1.02×10^{-8}. This experimental study shows that the proposed method could identify the location and magnitude of damage with good accuracy.

Fig. 18 shows the measured experimental force applied on the structure and a comparison of the measured acceleration with the reconstructed acceleration from the final updated structure of Scenario E2. The reconstructed acceleration is noted matching very closely with the measured values throughout the whole time history.

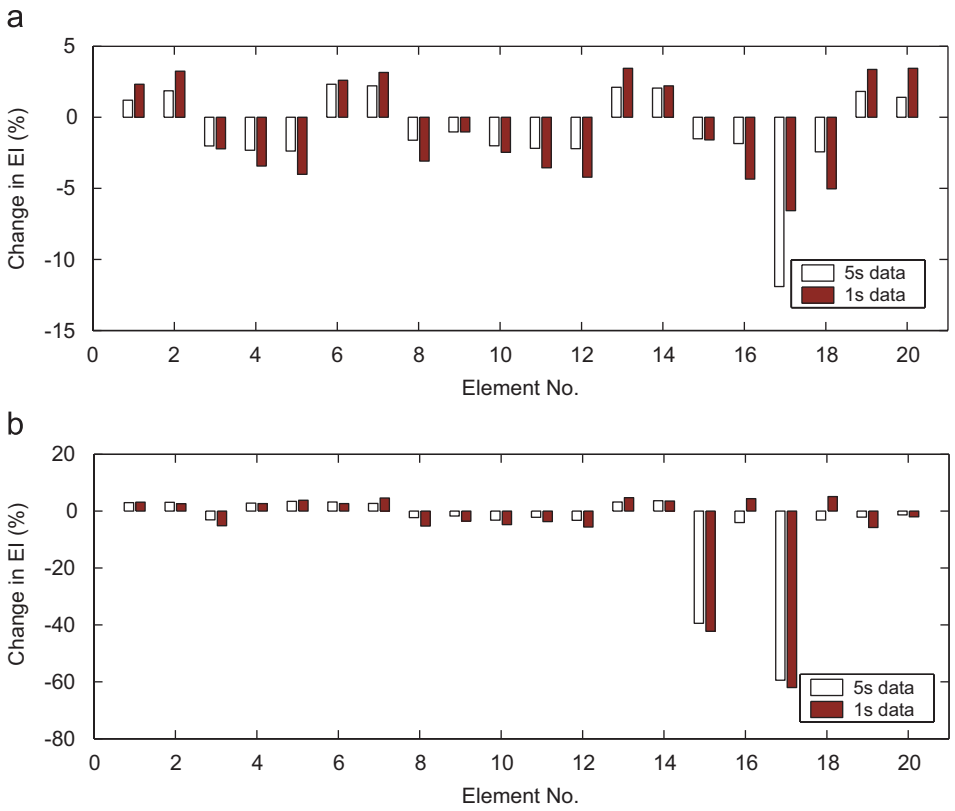

Fig. 17. Comparison on identified results using different number of measured data.

Table 5
Error (%) in the identified results in Scenarios $E1$ and $E2$

Element no.	Scenario $E1$	Scenario $E2$
1	1.2	3.01
2	1.87	3.11
3	−2.02	−3.06
4	−2.32	2.81
5	−2.37	3.43
6	2.32	3.21
7	2.21	2.68
8	−1.61	−2.28
9	−1.03	−1.72
10	−2.01	−3.16
11	−2.18	−2.18
12	−2.21	−3.22
13	2.11	3.19
14	2.05	3.64
15	−1.51	−3.31
16	−1.85	−4.02
17	1.02	−4.34[a]
18	−2.43[a]	−3.12
19	1.82	−2.13
20	1.41	−1.32

[a]Denote the largest value in the group.

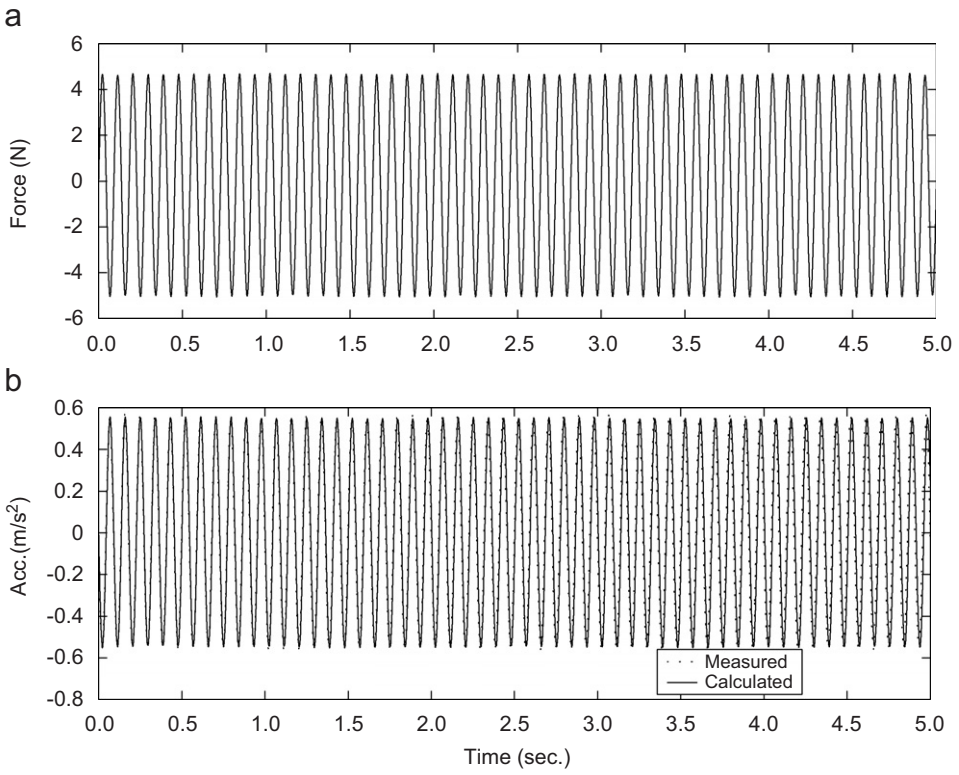

Fig. 18. (a) The measured excitation force, and (b) comparison on the measured and reconstructed accelerations from the updated structure.

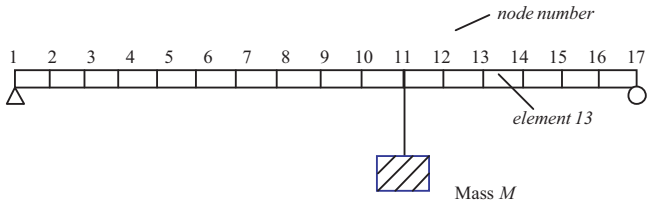

Fig. 19. Experimental set-up.

5.2. A simply supported steel beam

The proposed method is further demonstrated with another laboratory work on a simply supported steel beam as shown in Fig. 19. The parameters of the beam are: length 2.0 m, width 25 mm and height 19 mm, the elastic modulus and mass density of the material are 2.065×10^{11} N/m^2 and 7.832×10^3 kg/m^3 respectively. It is discretized into sixteen Euler beam elements with three dof at each node. A mass of 2.61 kg is hanged by a fine nylon rope at node 11 of the beam, and the excitation generated by cutting the rope will serve as the input force. The true value of the force is 25.58 N and is an "impulsive force" acting at the initial time $t = 0$. Mathematically, it is expressed as

$$f(t) = \begin{cases} Mg, & t = 0, \\ 0, & t > 0. \end{cases}$$

The flexural rigidities of all the elements and the assumed impulsive force are taken as the unknowns in the inverse analysis. The initial values of the damage parameters for all the finite elements are all zero.

A commercial data logging system INV303 and the associated signal analysis package DASP2003 are used in the data acquisition. The sampling frequency is 2000 Hz. A modal test was conducted on the intact beam as well as after a damage was introduced into the beam. The damage is introduced by removing equal thickness of 0.5 mm material from both sides of the beam over a length of 9 mm in element 13, with one edge of the damage zone starting at node 13. The first five natural frequencies of the undamaged beam are 10.523, 41.316, 92.615, 165.353, and 254.625 Hz, and those for the damaged beam obtained from the modal test are 10.282, 40.508, 91.264, 164.695 and 250.583 Hz. The impact test described above was conducted on the beam for identifying the damage.

Two acceleration responses collected by B&K 4370 accelerometers at nodes 7 and 9 of the beam were used for damage detection. 2000 data obtained from the two accelerometers from 0.5 to 1.5 s after the application of excitation were used for the identification. The first 0.5 s data was skipped because of the many high frequency components in the response caused by the impulsive force generated by the falling weight. The equivalent reduction in the flexural rigidity of element 13 is found to be 11.3% after reducing the middle dof to the two end nodes 13 and 14 by Guyan reduction.

The required number of iteration for convergence in the damage identification is 134, and the corresponding optimal regularization parameter is 11.36. Fig. 20 shows the identified flexural rigidities, and the reduction in element 13 is 12.9% which is close to the true value. But there is a large false alarm in element 12. This observation can be explained since element 12 is immediately adjacent to the damage and the vibration energy in the element would be much more disturbed than those in other elements as discussed by Shi and Law [30]. Fig. 21 shows the time histories of the reconstructed acceleration and the corresponding measured acceleration smoothed with twenty terms orthogonal polynomial function to remove the measurement noise [31]. The time series match each other very well. The natural frequencies of the beam calculated with the identified parameters are 10.268, 40.734, 92.251, 164.701 and 253.219 Hz which also match the experimental frequencies very well indicating the success of the identification.

6. Discussions

There are several important aspects of the proposed approach which cannot be covered in the studies above are discussed in the followings:

- The computation of the dynamic response and its sensitivity is based on the Newmark method. Yet there are other numerical methods or analytical method [32] by which the sensitivities can be obtained. The numerical approach has a lower limit of sampling rate below which the accuracy of computation will be affected [32].
- The excitation input using a dynamic hammer is only suitable for laboratory test. For large practical structure where a large amount of input energy is required to have sufficient excitation of the structure, natural excitation such as ground-borne excitation [33] or vehicular excitation [34,35] would be more appropriate.

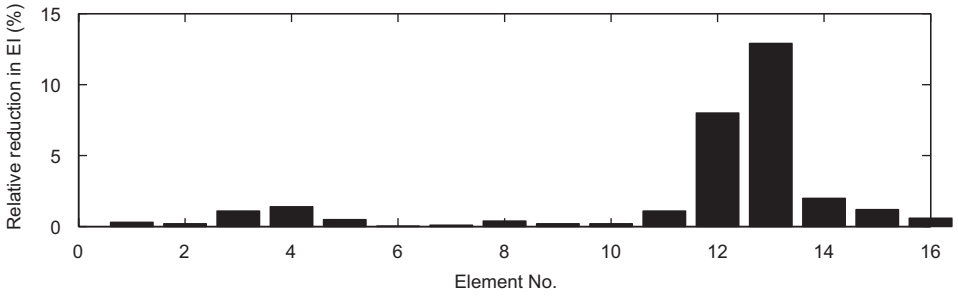

Fig. 20. Identified change in flexural rigidity in the experimental beam.

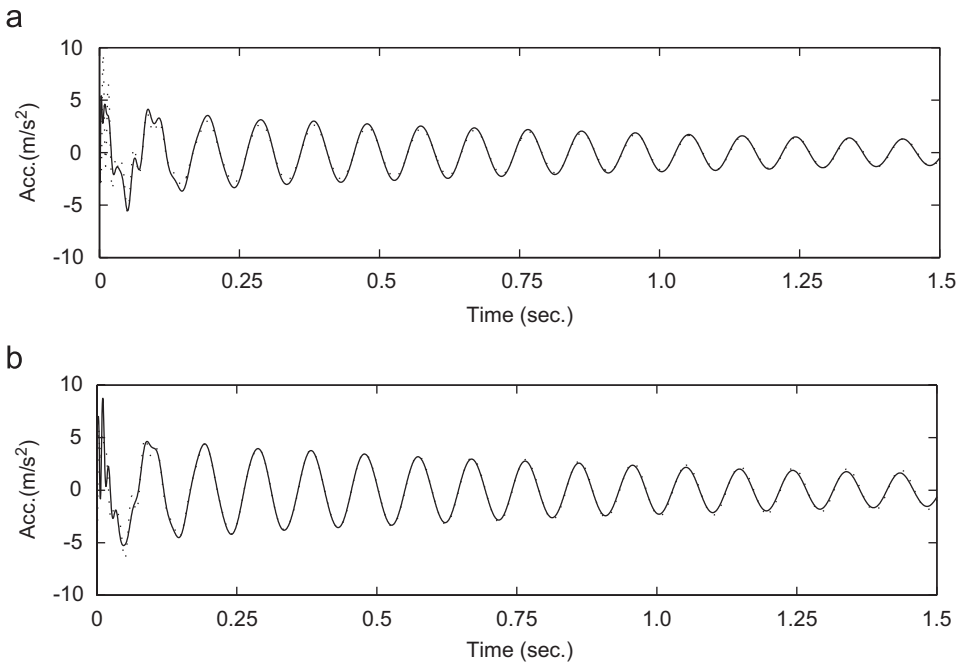

Fig. 21. Comparison of measured and reconstructed acceleration response from the simply supported beam: (a) from Node 7; (b) from Node 9; ___ calculated; …… experiment.

- Initial model error and random measurement noise are two most significant factors influencing the accuracy of any damage detection algorithm. Their effect can, however, be quantified or limited if only one of them exist [36]. The error due to the model error, would however, be amplified if both of them are present, and therefore a two-stage approach for the damage detection is usually adopted with the first stage to identify the initial model error and the next stage to identify the local changes in the structure. This approach has been adopted in the present study.
- Accurate damage detection not only requires an effective algorithm of computation, but also an appropriate model description on the target damage such that a relevant parameter can be taken as the unknown in the identification. The most general form of damage description of a change in the elastic modulus of material has been adopted in the simulation study to illustrate the effectiveness of the proposed approach, while more accurate description of the crack damage and the removal of material in the experiments have been used to illustrate the accuracy of the proposed approach.
- The proposed approach takes advantage of the plentiful measured data in the response time history to formulate an over-determined set of equations for the damage detection. The information obtained from a sensor location is limited in the modal-based approach. But with the present response-based approach, each response data at one discretized time instance forms one equation in the optimization. The over-determined set of equations can be formed easily from even one measured location. Fig. 17 shows that the identified results obtained from using 5 s of data are much better than those obtained from using 1 s of measured response. The optimal combination of sensor locations and optimal sensor number, however, needs to be studied but with some new technique and objective function which differ from what we have with modal parameter based identification techniques.

7. Conclusions

Sensitivity of general dynamic response of a structure with respect to a perturbation of a system parameter is studied. Sinusoidal excitation is shown better than the impulsive excitation or random excitation to give higher sensitivity with the presented simulation examples. A novel damage identification method based on

dynamic response sensitivity is proposed. The sensitivity matrix of the dynamic response with respect to a system parameter is calculated, and it is used in a sensitivity-based method to update the parameters using measurement from two states of the structure. This approach involves measurement error while the different modeling errors of the system can be identified iteratively taking advantage of the plentiful measured data. Although only one or two response measurement are involved for the examples studied, more accurate results can be obtained when longer durations of measurement are included in the identification. This study also shows that acceleration measurement seems to give better identified results than displacement measurement.

Acknowledgements

The work described in this paper was supported by a research grant from the Hong Kong Polytechnic University.

References

[1] P. Cawley, R.D. Adams, The location of defects in structures from measurements of natural frequencies, *Journal of Strain Analysis* 14 (1979) 49–57.
[2] N. Bicanic, H.P. Chen, Damage identification in framed structures using natural frequencies, *International Journal for Numerical Methods in Engineering* 40 (1997) 4451–4468.
[3] H.P. Chen, N. Bicanic, Assessment of damage in continuum structures based on incomplete modal information, *Computers and Structures* 74 (2000) 559–570.
[4] C. Farhat, F.M. Hemez, Updating finite element dynamic models using an element-by-element sensitivity methodology, *AIAA Journal* 31 (1993) 1702–1711.
[5] J.V. Araujo Dos Santos, C.M. Mota Soares, C.A. Mota Soares, H.L.G. Pana, Development of a numerical model for the damage identification on composite plate structure, *Composite Structures* 48 (2000) 59–65.
[6] D. Wu, S.S. Law, Model error correction from truncated modal flexibility sensitivity and generic parameters. I: Simulation, *Mechanical Systems and Signal Processing* 18 (6) (2004) 1381–1399.
[7] Z.Y. Shi, S.S. Law, L.M. Zhang, Structural damage detection from modal strain energy change, *Journal of Engineering Mechanics, ASCE* 126 (12) (2000) 1216–1223.
[8] S. Hassiotis, G.D. Jeong, Assessment of structural damage from natural frequency measurements, *Computers and Structures* 49 (1993) 679–691.
[9] A.M. Kabe, Stiffness matrix adjustment using modal data, *AIAA Journal* 23 (1985) 1431–1436.
[10] T.W. Lim, Structural damage detection of space truss structures using best achievable eigenvectors, *AIAA Journal* 32 (1994) 1049–1057.
[11] D.C. Kammer, A hybrid approach to test-analysis model development for large space structures, *Journal of Vibration and Acoustic* 113 (1991) 325–332.
[12] J.M. Ricles, J.B. Kosmatka, Damage detection in elastic structures using vibratory residual forces and weighted sensitivity, *AIAA Journal* 30 (1992) 2310–2316.
[13] Z. Li, S.M. Xia, J. Wang, X.Y. Su, Damage detection of cracked beams based on wavelet transform, *International Journal of Impact Engineering* 32 (7) (2006) 1190–1200.
[14] X.Q. Zhu, S.S. Law, Wavelet-based crack identification of bridge beam from operational deflection time history, *International Journal of Solids and Structures* 43 (7–8) (2006) 2299–2317.
[15] U.P. Poudel, G. Fu, J. Ye, Structural damage detection using digital video imaging technique and wavelet transformation, *Journal of Sound and Vibration* 286 (4–5) (2005) 869–895.
[16] A.V. Ovanesova, L.E. Suárez, Applications of wavelet transforms to damage detection in frame structures, *Engineering Structure* 26 (1) (2004) 39–49.
[17] L.H. Yam, Y.J. Yan, J.S. Jiang, Vibration-based damage detection for composite structures using wavelet transform and neural network identification, *Composite Structures* 60 (4) (2003) 403–412.
[18] Q. Sun, Y. Tang, Singularity analysis using continuous wavelet transform for bearing fault diagnosis, *Mechanical Systems and Signal Processing* 16 (6) (2002) 1025–1041.
[19] I. Sheinman, Damage detection and updating of stiffness and mass matrices using mode data, *Computer and Structures* 59 (1) (1996) 149–205.
[20] D.C. Zimmerman, M. Kaouk, Structure damage detection using a minimum rank updating theory, *Journal of Vibration and Acoustics* 116 (1994) 222–253.
[21] G.R. Liu, S.C. Chen, A novel technique for inverse identification of distributed stiffness factor in structures, *Journal of Sound and Vibration* 254 (5) (2002) 823–835.
[22] K. Balasubramaniam, N.S. Rao, Inversion of composite material elastic constants from ultrasonic bulk wave phase velocity data using genetic algorithms, *Composite: Part B* 29B (1998) 171–180.

[23] J. Cunha, S. Cogan, C. Berthod, Application of genetic algorithm for the identification of elastic constrains of composite materials form dynamic tests, *International Journal for Numerical Methods in Engineering* 45 (1999) 891–900.
[24] G.R. Liu, S.C. Chen, Flaw detection in sandwich plates based on time-harmonic response using genetic algorithm, *Computers Methods in Applied Mechanics and Engineering* 190 (2001) 5505–5514.
[25] K.J. Bathe, *Finite Element Procedures in Engineering Analysis*, Prentice Hall, New Jersey, 1982.
[26] M.I. Friswell, J.E. Mottershead, *Finite Element Model Updating in Structural Dynamics*, Kluwer Academic Publisher, Dordrecht, The Netherlands, 1995.
[27] A.M. Tikhonov, On the solution of ill-posed problems and the method of regularization, *Soviet Mathematics* 4 (1963) 1035–1038.
[28] P.C. Hansen, Analysis of discrete ill-posed problems by means of the L-curve, *SIAM Review* 34 (4) (1992) 561–580.
[29] J.K. Sinha, M.I. Friswell, S. Edwards, Simplified models for the location of cracks in beam structures using measured vibration data, *Journal of Sound and Vibration* 251 (1) (2002) 13–38.
[30] Z.Y. Shi, S.S. Law, L.M. Zhang, Structural damage detection from modal strain energy change, *Journal of Engineering Mechanics, ASCE* 126 (12) (2000) 1216–1223.
[31] X.Q. Zhu, S.S. Law, Orthogonal function in moving force identification on a continuous beam, *Journal of Sound and Vibration* 245 (2) (2001) 329–345.
[32] S.S. Law, Z.R. Lu, State space approach to calculate the sensitivity of dynamic response, *Symposium on Advances in System Identification Techniques Technical Committee on Vibration and Sound*, ASME Design Engineering Division Dynamics and Control of Structures & Systems committee, ASME Applied Mechanics Division, Anaheim Convention Center/Hilton Anaheim, CA, USA, November 14–19, 2004.
[33] X.Y. Li, S.S. Law, Structural damage detection with statistical analysis from support excitation, *Journal of Engineering Mechanics, ASCE*, under review.
[34] Z.R. Lu, S.S. Law, System identification including the load environment, *Journal of Applied Mechanics, ASME* 71 (5) (2004) 739–741.
[35] X.Q. Zhu, S.S. Law, Damage detection in simply supported concrete bridge structures under moving vehicular loads, *Journal of Vibration and Acoustics, ASME* 129 (1) (2007) 58–65.
[36] S.S. Law, X.Y. Li, Z.R. Lu, Structural damage detection from wavelet coefficient sensitivity with model errors, *Journal of Engineering Mechanics, ASCE* 132 (10) (2006) 1077–1087.